Int. J. Electrochem. Sci., 16 **(2021)** Article ID: 21063, doi: 10.20964/2021.06.34

International Journal of
ELECTROCHEMICAL
SCIENCE
www.electrochemsci.org

Fabrication of WO_3/Al_2O_3 Composite Ceramic Coatings on 6063 Aluminum Alloy by Ultrasound-enhanced Micro-Arc Oxidation

Yupeng Guo[1,*], *Zhenguo Wei*[1], *Dongbo Wei*[2], *Daqiang Ma*[1], *Xiaofeng Lu*[1], *Xiaolei Zhu*[1]

[1] School of Mechanical and Power Engineering, Nanjing tech university, Nanjing 211816, China
[2] School of Mechatronic Engineering, Harbin Institute of Technology, Harbin150001, China
[*]E-mail: guoyupeng@njtech.edu.cn

Received: 23 December 2020 / *Accepted:* 16 March 2021 / *Published:* 30 April 2021

WO_3/Al_2O_3 composite ceramic coatings were prepared through ultrasound-enhanced MAO technique on 6063 aluminum substrates. The hardness and corrosion performance of the substrate were improved. The diameter of micropores on the surface of the coatings decreased with increasing Na_2WO_3 concentration. X-ray diffraction results showed the coatings consisted of γ-Al_2O_3, α-Al_2O_3, and WO_3. The amounts of γ-Al_2O_3 and WO_3 increased with increasing Na_2WO_3 concentration. The roughness decreased from 2.00μm to 1.67μm. The corrosion current density reduced from 32.59μA/cm^2 to 0.29μA/cm^2, and the hardness increased from 1025HV to 1465HV. The vibration amplitude of the electrolyte increased with increasing ultrasonic power and reached 144μm at 700W, which changed the microstructure of the coatings.

Keywords: Ultrasound enhanced micro-arc oxidation, ceramic coatings, corrosion performance

1. INTRODUCTION

Aluminum and aluminum alloy are widely used in aviation, naval, and other fields due to their low density and high strength[1, 2]. However, the surface property[3, 4] and hardness of these materials limit their application[5]. Ultrasonic-enhanced micro arc oxidation (MAO)[6, 7], as a new surface treatment technology, has gained increasing attention for preparation of ceramic coatings. He[8] studied the effect of ultrasonic composite MAO on the growth of A96061 aluminum alloy coatings; the method improved the growth behavior and anti-vibration performance of the coatings. Shen[9] evaluated the effect of ultrasonic composite MAO on 6061 aluminum alloy coatings. Ultrasound effectively promoted the formation of α-Al_2O_3, reduced the formation of larger discharge micro pores, and increased the coating thickness. Qu[10] investigated ultrasound-MAO treatment of magnesium alloys for medical use, the polarization resistance was the optimal 120W ultrasound power. However, the vibration of ultrasound

at low power was small, and the effect on the MAO discharge process may be limited. Quantitative analysis of the relationship between ultrasonic power and the vibration of electrode was found to be a key factor for analysis of ultrasonic process. Quantitative measurement of ultrasonic vibration has not been evaluated yet. Na_2WO_4 is typically used to improve the friction and corrosion properties of coatings in MAO[11, 12]. Chen[13] determined the effect of Na_2WO_4 on the MAO coatings of the Al-Ti double component. Na_2WO_4 enhanced the intensity of the reaction and increased the thickness of the coatings. Chen[14] used Na_2WO_3 to improve the polarization resistance of MAO-coated Mg-Zn-Ca alloy; the optimal combination comprised 0.5 g/L Na_2WO_4 and other additives. Hakimizad[15] studied the pulse current mode on the plasma electrolytic oxidation of 7075 Al in Na_2WO_4-containing solution; the hardness of the coatings was improved to 1900HV. Bayati[16] studied the characteristics and coating formation mechanism of WO_3 and TiO_2 nanocomposite coatings produced by different treatment voltages; the band gap energy of the coatings was estimated to be 2.87eV, and the degradation rates were 2.210^{-2} and 0.910^{-2} min^{-1}, respectively.

Considering the successful application of Na_2WO_4 to MAO, Na_2WO_4 was used to prepare WO_3/Al_2O_3 ceramic coatings through ultrasound-enhanced MAO; this method could be used to expand the applications of MAO technology in corrosive environments. In the current work, WO_3/Al_2O_3 ceramic coatings were prepared with different Na_2WO_4 concentrations under ultrasound. The relationship among ultrasound power, concentration of Na_2WO_3, microstructure, morphology, corrosion property, hardness of the coatings was studied.

2. MATERIALS AND METHOD

2.1. Preparation of MAO coatings

Circular aluminum alloy sample with a diameter of 15 mm and a thickness of 2 mm was used. The chemical element composition of the samples was AlMgSi (Wt %): Mg 0.45 %–0.9 %, Si 0.2 %–0.6 %, Cu ≤ 0.1 %, Fe ≤ 0.35 %, Mn ≤ 0.1 %, Zn ≤ 0.1 %, Cr ≤ 0.1 %, Ti ≤ 0.1 %, and Al. The samples were polished with 800× 2000 # SiC sand paper and washed with ethanol. The experiments were carried out after drying. The MAO equipment was composed of 10 kW MAO power supply (independently developed by Nanjing tech university), stainless steel sink, and cooling system. The sample was connected to the positive pole of the power supply as the anode. Stainless steel sink was used as the cathode. The ultrasonic equipment was JH-10000, the power was 900W, and the frequency was 28kHz. The electrolytic cell was placed inside the ultrasonic cell, and the ultrasonic cell, which was filled with water. The ultrasonic vibration was transmitted to the steel sink through water. The working solution was composed of Na_2SiO_3, KOH, Na_2WO_3, and deionized water. The concentration of Na_2SiO_3 was 4g/L, and that of KOH was 4g/L. The power supply and process parameters for preparing the coatings are shown in Table 1. The substrate was AlMgSi and the coatings were defined as AlMgSi-1, AlMgSi-2, AlMgSi-3, AlMgSi-4, AlMgSi-5, AlMgSi-6. The temperature of the electrolyte was maintained at 30℃–35℃ by using a stirring pump. According to previous experiments[17-19], the frequency, duty

cycle, and time were set to 500 Hz, 50%, and 35 min, respectively. In constant voltage mode, the processing voltage was 520 V.

Table 1. the chemical composition, electrical conductivity and pH of the electrolyte under 500 Hz, 50% duty cycle, and 35 min

Sample No.	Ultrasound Power (W)	Na_2SiO_3 (g/L)	KOH (g/L)	Na_2WO_3 (g/L)	Electrical conductivity (mS/cm,24°)	pH
AlMgSi-1	0	4	3	0	10.08	12.1
AlMgSi-2	0	4	3	1	10.74	12.1
AlMgSi-3	700	4	3	1	10.74	12.1
AlMgSi-4	700	4	3	2	10.93	12.1
AlMgSi-5	700	4	3	3	11.25	12.1
AlMgSi-6	700	4	3	4	11.56	12.1

2.2. Analysis of structure and composition of the coatings

The microstructure of the coatings was analyzed using JSM-6480A scanning electron microscope (SEM) and EDS. The phase structure of the specimens was detected using D/max-r B X-ray diffraction (XRD, Cu Kα radiation). The scattering angle 2θ was set from 10° to 90° with a step of 0.041°, an acquisition time of 1 s/step, energy of 40 kV, and current of 40 mA. PHI5700ESCA System X-ray photoelectron spectroscopy (XPS, twin anode, X-ray source, using Al Ka α¼1 486.6eV) was employed to probe the surface chemical composition and valence of the samples. The surface roughness of the coatings was measured using a roughness tester (TR200, cut-off length 0.8 mm). The surface hardness of the coatings was evaluated using a digital micro-hardness tester (HVS-1000) in HV mode at a load of 25 g for 5 s. The electrochemical workstation CHI604C was employed to detect the corrosion property of the specimens through Tafel testing with an initial potential of −2V, a final potential of 1V, a quiet time of 200 s, and a scan rate of 1mV/s. Three-electrode cell set-up was used in which the prepared sample was the working electrode and a platinum sheet and a saturated calomel electrode were used as the counter and reference electrodes, respectively. The experiments were performed in 3.5 wt.% NaCl solution at room temperature. Ultrasonic vibration was used displacement detection system (independently developed by Nanjing tech-university), the laser displacement sensor was HG-C1000, with a measurement range of 3mm and an accuracy of 1μm. Vibration signal was collected by UPO2104CS oscilloscope.

3. RESULTS AND DISCUSSION

3.1 SEM

The ultrasonic power and concentration on the microstructure of the coatings are shown in Figure 1. Uniform MAO coatings were obtained on the substrates (Figure 1a). The surface of the coatings contained micro pores and molten regions which were formed due to the heating, melting, and quenching

of the molten oxides[20]. Smooth areas appeared on the coatings under 1 g/L Na_2WO_3 (Figure 1b). WO_3^{2-} in the electrolyte participated in the MAO reaction and changed the morphology of the coatings. A dense "stack" was generated under ultrasonic-enhanced MAO (Figure 1c). The ultrasonic waves produced high-frequency oscillations in the electrolyte, which caused the oscillation of electrolyte around the spark discharge channel.

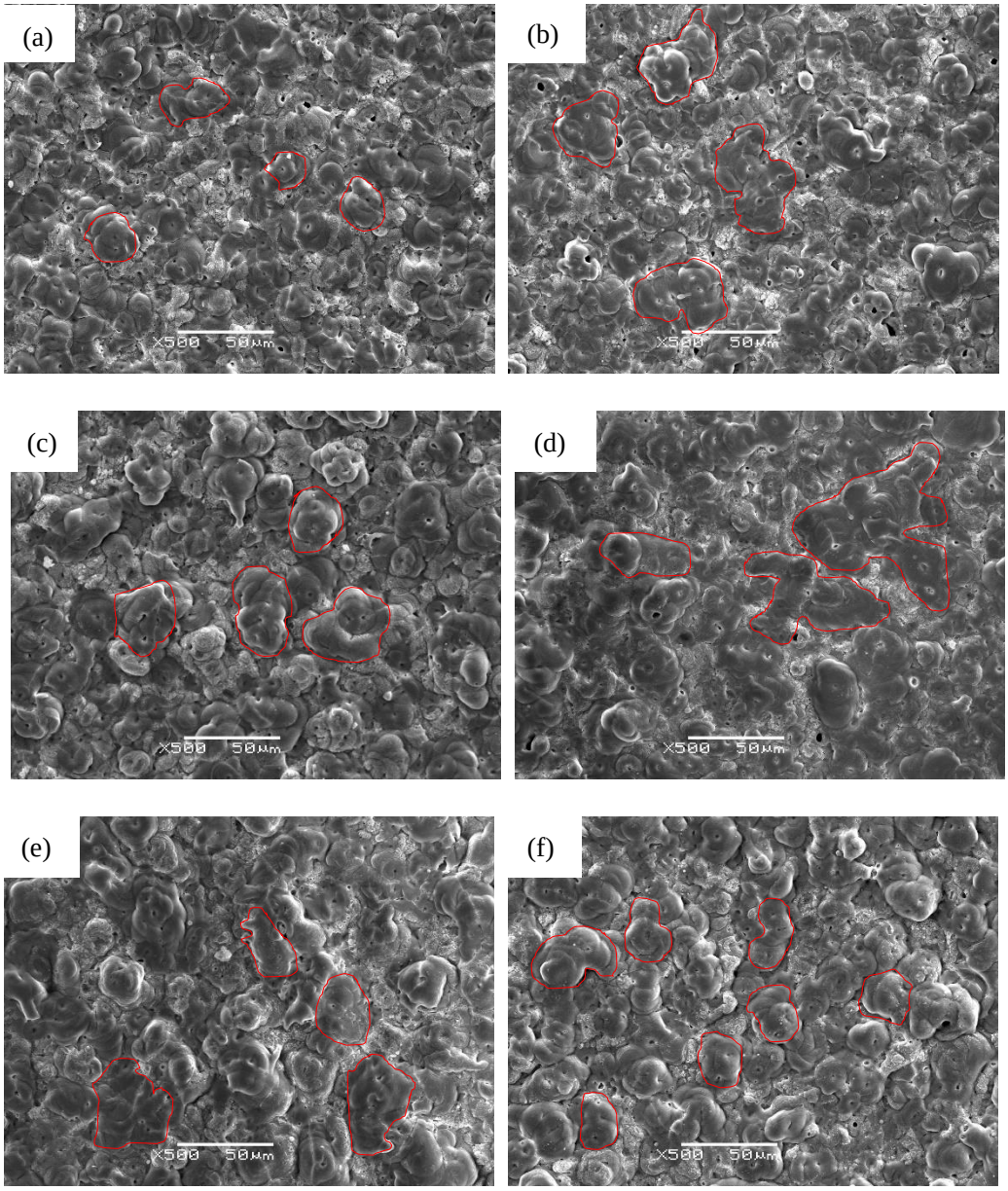

Figure 1. the ultrasonic power and concentration on the microstructure of the coatings (a)AlMgSi-1; (b)AlMgSi-2; (c)AlMgSi-3; (d)AlMgSi-4; (e)AlMgSi-5; (f)AlMgSi-6;

The high oscillation frequency of the electrolyte induced the production of cold quenching by the spark discharge channel of MAO, which generated a dense "stack" and promoted the reduction of diameter on the generated small holes. With increasing Na_2WO_3 concentration, the "stack" of the coatings gradually decreased, the smooth areas appeared, and the number of micropores decreased. WO_3

was distributed more evenly on the coatings, and their morphology was smooth under ultrasonic treatment. However, the dense "stack" on the surface of the coatings indicated the high concentration of Na_2WO_3 at AlMgSi-6 (Figure 1f), which may affect the performance of the coatings.

3.2 Cross section

The cross section of the coatings is shown in Figure 2. The thickness of the coatings increased from 35 μm to 39 μm with increasing Na_2WO_3 concentration under ultrasound treatment (Figure 2b). Ultrasonic vibration promoted the process of MAO and increased the thickness of the coatings. The WO_3^{2-} ions moved to the anode under the action of electric field and participated in micro arc discharge, leading to the formation of WO_3. The content of WO_3 and the thickness of the coatings increased with increasing concentration of WO_3^{2-} ion.

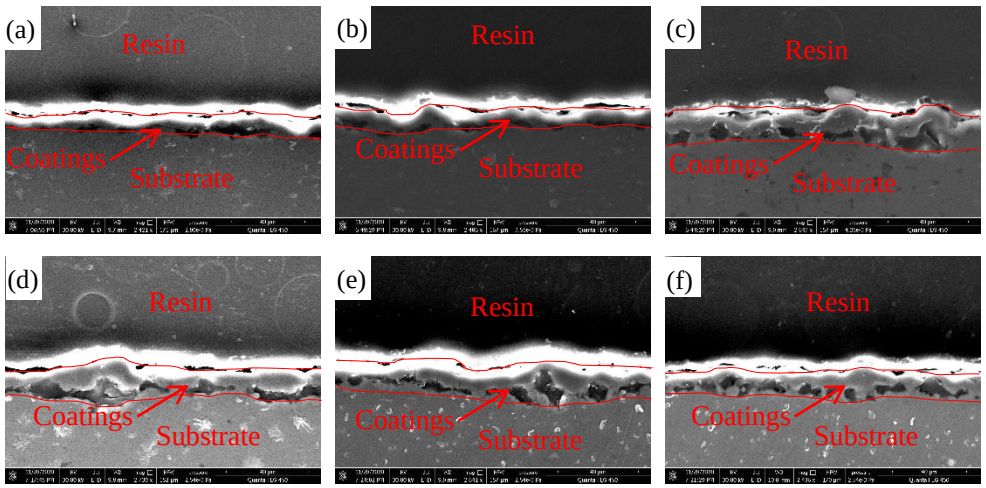

Figure 2. Cross section of the coatings under different preparation conditions (a)AlMgSi-1; (b)AlMgSi-2; (c)AlMgSi-3; (d)AlMgSi-4; (e)AlMgSi-5; (f)AlMgSi-6;

3.3 EDS

The EDS results of the coatings under different preparation conditions are shown in Table 2. The coatings were composed of O, Mg, Al, Si, and W. Si was obtained from Na_2SiO_3, and W was derived from Na_2WO_3. Al and Mg were obtained from the Al substrates, and O was derived from the Al_2O_3 ceramic coatings. The W content was 1.14 % at AlMgSi-2, which generated WO_3. WO_3^{2-} in the electrolyte participated in the MAO reaction and entered into the coatings. The W content was 1.36 % under ultrasonic addition, which promoted the MAO and increased the content of W. The content of W was increased from 1.14 % to 2.30 % with increasing Na_2WO_3 concentration.

Table 2. the EDS of surface scanning results under different preparation conditions

No.	O (At%)	Mg (At%)	Al (At%)	Si (At%)	W (At%)
AlMgSi-1	30.97	0.31	61.79	6.93	0
AlMgSi-2	30.59	0.16	60.92	6.71	1.14
AlMgSi-3	31.89	0.52	58.10	7.55	1.36
AlMgSi-4	30.48	0.43	56.57	10.55	1.65
AlMgSi-5	32.87	0.30	54.52	9.89	1.91
AlMgSi-6	31.66	0.29	57.09	8.16	2.30

3.4 XRD

The XRD patterns of the coatings obtained under different preparation conditions are shown in Figure 3. The coatings consisted of γ-Al_2O_3, α-Al_2O_3, and WO_3. X-rays penetrated the coatings because they were thin. γ-Al_2O_3 appeared in the XRD diffraction peak at AlMgSi-2, illustrating that Na_2WO_3 increased the thickness of the coatings. The γ-Al_2O_3 peak value of XRD was further increased at AlMgSi-3, and ultrasound promoted the MAO reaction, as discussed in section 3.9. The peak intensities of γ-Al_2O_3 and WO_3 gradually increased with increasing Na_2WO_3 concentration which illustrated the WO_4^{2-} participated in the formation of the MAO coating[21]. A trace of α-Al_2O_3 appeared on the coatings. The diffraction peak of WO_3 coincided with the diffraction peak of Al_2O_3 [22], and the peak intensity gradually increased, indicating that WO_3 entered the coatings during the MAO process. However, the peak intensity of WO_3 at 23.966° was lower due to the low content of WO_3 given that the highest content was 2.30 % in the EDS analysis. Na_2WO_3 was separated into Na^+ and WO_4^{2-} in the electrolyte, and a chemical reaction was carried out during the process: $2WO_4^{2-} - 4\ e^- = 2WO_3 + O_2\uparrow$. WO_3 was obtained by the MAO treatment.

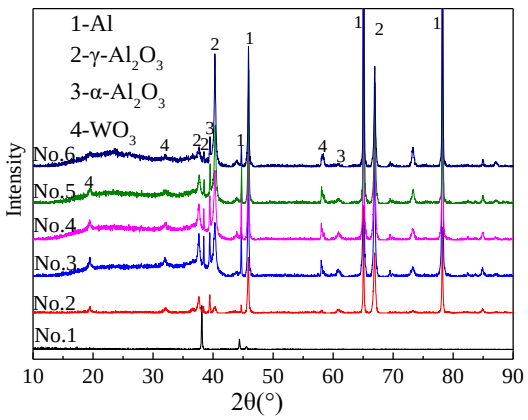

Figure 3. XRD of the coatings prepared under different ultrasonic power and concentration (1) AlMgSi-1; (2) AlMgSi-2; (3) AlMgSi-3; (4) AlMgSi-4; (5) AlMgSi-5; (6) AlMgSi-6;

3.5 XPS

XPS analysis was conducted to determine the valence and chemical composition of the coatings (Figure 4). A core-level binding energy of 285.0 eV for electrolyte C1s was used as reference to explain

the results. The wide-scanning results show that the coatings were composed of Al(2p), O(1s), Si(2p), and W(4f) (Figure 4a); this finding is consistent with the results of XRD and EDS analyses. The core-level binding energy of Al(2p) is depicted in Figure 4b). The peak at binding energy of 70.7 eV, corresponds to Al-O bonds in Al_2O_3[23]. The O(1s) core-level binding energy is depicted in Figure 4c), which is represented by two distinct peaks. Peak A at binding energy of 529.2 eV corresponds to Al-O bonds in Al_2O_3[24],Si-O bonds and W-O bonds. Peak B, at binding energy of 528.2 eV corresponds to oxygen in O–H groups [25, 26]. The peak at binding energy of 32.68 eV corresponds to W-O bonds in WO_3. Peak B at binding energy of 34.69 eV corresponds to some non-stoichiometric tungsten oxides W-O bonds in W_xO_y[27]. W tended to appear primarily in the outer and inner regions of the coating, and originated from the electrophoresis and diffusion of the electrolyte solution through the pores in the coatings. These experimental results were in good agreement with the XRD analysis.

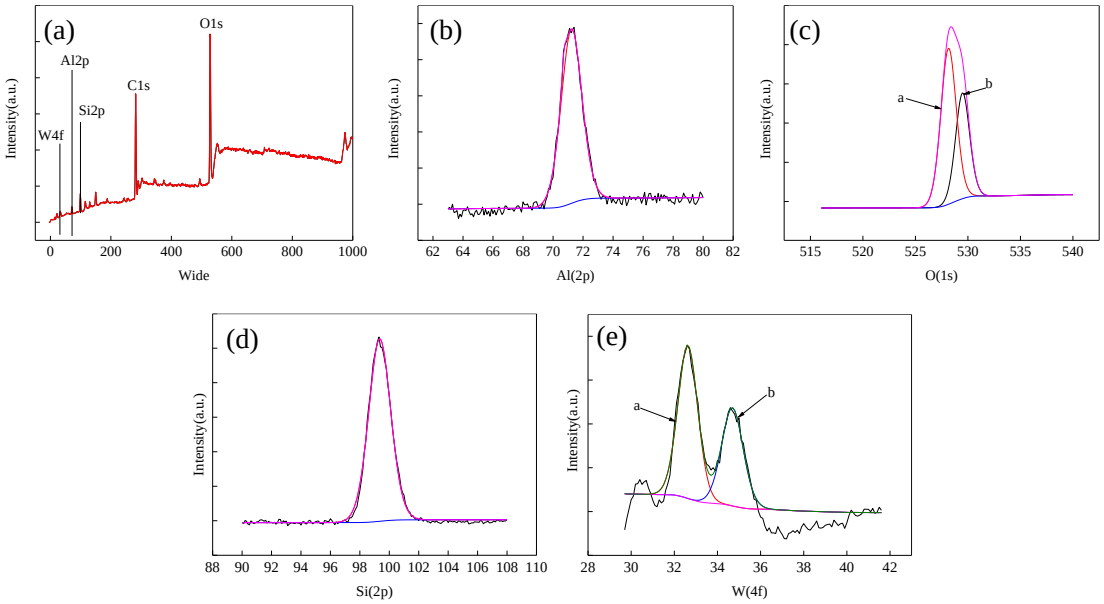

Figure 4. XPS of the coatings at AlMgSi-5 (a) Wide (b) Al(2p) (c) O(1s) (d) Si(2p) (f) W(4f)

3.6 Roughness

The surface roughness of the coatings obtained under different preparation conditions are shown in Figure 5. The surface roughness decreased from 1.34μm to 1.25μm at 1 g/L Na_2WO_3. The SEM results show the coatings had smooth area after the addition of Na_2WO_3. After ultrasonic treatment at AlMgSi-3, the roughness was increased to 2.00μm, because the stack increased. With increasing Na_2WO_3 concentration, the roughness of the coatings decreased from 2.00μm to 1.67μm. The content of Na_2WO_3 increased, and a smooth region appeared on the surface of the coatings, which reduced the roughness.

3.7 Corrosion property

The anticorrosive performance of the coatings is shown in Figure 6 and Table 3. The corrosion current density was reduced from 32.59μA/cm^2 to 1.88μA/cm^2 after MAO treatment. Because of the

effect of ultrasonic wave, the loose layer was removed and the dense layer was more compact, the polarization resistance of ultrasonic MAO coatings were better than that of single MAO coatings[28].

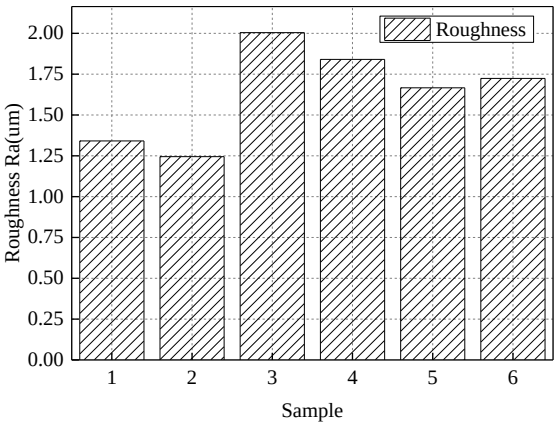

Figure 5. Roughness of the coatings under different preparation conditions (1) AlMgSi-1; (2) AlMgSi-2; (3) AlMgSi-3; (4) AlMgSi-4; (5) AlMgSi-5; (6) AlMgSi-6;

The treatment improved the polarization resistance of the AlMgSi. The corrosion current density of the MAO coatings was improved to 1.70μA/cm^2 by Na_2WO_3, indicating Na_2WO_3 improved the anticorrosive performance. The increase in the coating thickness and γ-Al_2O_3 content improved the anticorrosive performance. With increasing Na_2WO_3 concentration, the corrosion current density gradually decreased from 2.50μA/cm^2 to 0.29μA/cm^2. Under the effect of ultrasonic vibration, the content of WO_3 on the coatings was increased, which improved the polarization resistance. The anticorrosive property of the ceramic coatings was decided by microstructure and chemical composition, etc.[10]. The ultrasonic was improved the SEM and EDS as shown in Figure 2 and table 2. The increase in the Al_2O_3 content improved the polarization resistance of the coatings. The thickness of the coatings was increased, leading to difficulty of the corrosion solution in penetrating the coatings. However, the corrosion current density was increased to 0.41μA/cm^2 at AlMgSi-6, the concentration of Na_2WO_3 was too high, which influenced the SEM morphology (Figure 1f).

Table 3. Corrosion potential, corrosion current density and polarization resistance of the coatings tested in 3.5% NaCl solution

NO.	Corrosion potential (V)	Corrosion current density (μA/cm^2)	Polarization resistance (R)
AlMgSi-1	-0.598	1.88	21798.9
AlMgSi-2	-0.384	1.70	30816.3
AlMgSi-3	-0.238	2.50	17376.5
AlMgSi-4	-0.128	0.22	210612.6
AlMgSi-5	-0.195	0.29	127665.1
AlMgSi-6	-0.110	0.41	75119.5
AlMgSi	-0.871	32.59	1298.8

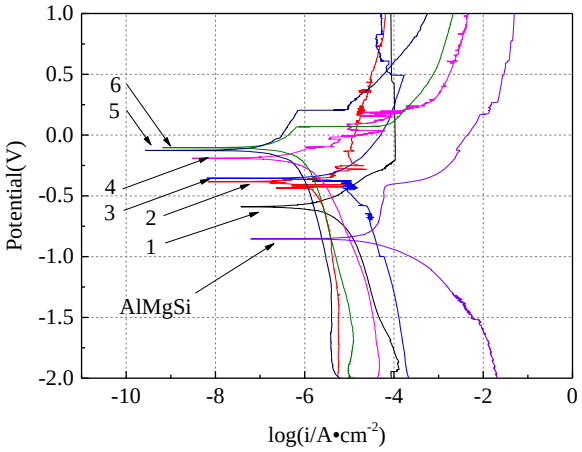

Figure 6. Potentiodynamic polarization curves of the coatings tested in 3.5% NaCl solution (1) AlMgSi-1; (2) AlMgSi-2; (3) AlMgSi-3; (4) AlMgSi-4; (5) AlMgSi-5; (6) AlMgSi-6.

3.8 Hardness

Hardness of the coatings prepared under different conditions are shown in Figure 7. The hardness of 6063 aluminum alloy substrate is 83 HV [29] and improved by MAO. Na_2WO_3 increased the hardness of the coatings from 1025 HV to 1097 HV. The element W entered the coatings and generated WO_3, similar to the XRD results, thereby improving the hardness of the coatings. Na_2WO_3 changed the conductivity of the electrolyte (Table 1). More energy was applied to the growth of the coatings, and the Al_2O_3 content in the coatings increased, which increased the hardness of the coatings.

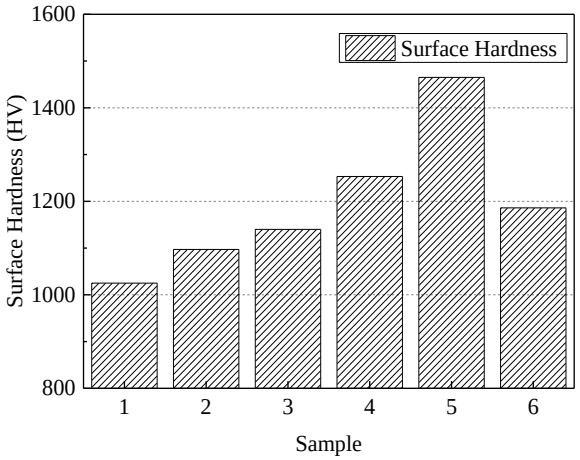

Figure 7. Hardness of the coatings prepared under different conditions (1) AlMgSi-1; (2) AlMgSi-2; (3) AlMgSi-3; (4) AlMgSi-4; (5) AlMgSi-5; (6) AlMgSi-6;

Ultrasonic-enhanced MAO increased the hardness of the coatings from 1097 HV to 1140 HV. Ultrasonic vibration promoted the cold quenching of the electrolyte, and the aluminum content in the coatings increased, leading to increased hardness. Under the action of ultrasound, the hardness of the coatings gradually increased to 1465 HV with increasing Na_2WO_3 concentration; the concentration of

Na_2WO_3, the content of WO_3 in the coatings and the content of γ-Al_2O_3 increased, thereby increasing the hardness of the coatings. Compared with the CeO_2 nano-particles doped in MAO coatings[19], the WO_3 was doped into the coatings and produced the WO_3/Al_2O_3 composite coatings, which improved the hardness of the coatings.

3.9 Mechanism of ultrasound enhanced MAO

A laser displacement sensor was used to measure the high-frequency vibration generated by ultrasound and clarify its role in the MAO process. Measurement of ultrasonic vibration under different ultrasound power are shown in Figure 8. As the ultrasonic power was increased, the vibration amplitude of the electrolyte increased, and the peak value caused by ultrasonic waves in the displacement curve increased. The displacement fluctuation was small, with an amplitude of 5μm without applying ultrasound. When the ultrasonic power was 100W, a sharp peak of vibration appeared on the displacement curve. The peak value was 20μm, and it was accompanied by low-frequency vibration. With increasing ultrasonic power, the amplitude of the high-frequency vibration spike increased. The amplitude increased from 45μm at 300W to 144μm at 700W with increasing low-frequency displacement amplitude.

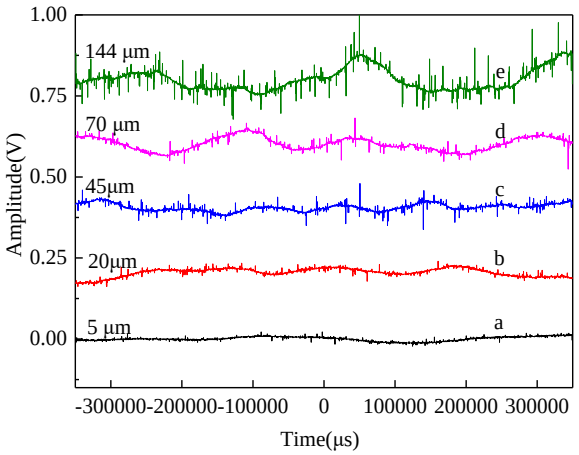

Figure 8. Measurement of ultrasonic vibration under different ultrasound power (a) 0 W, (b) 100 W, (c) 300 W, (d) 500 W, (e) 700 W

The introduction of ultrasound into the MAO process increased the high-frequency vibration process of the electrolyte, and the vibration frequency was 10 kHz. During the MAO process, electrolyte ions, such as SiO_3^{2-}, OH^-, and WO_3^{2-} ,migrated to the anode at the V_1 speed under the action of the stirring pump and electric field[30]. The reaction occurred at the end of the workpiece, and spark discharge was carried out. After applying ultrasound, the spark discharge time during MAO was about 1μs[31], and the single wave time of ultrasonic vibration was about 1μs, which effectively promoted the movement of the electrolyte[32]. SiO_3^{2-}, OH^-, and WO_3^{2-} obtained velocity V_2 under ultrasonic vibration, and the velocity toward the anode was V_1+V_2. Meanwhile, the vibration generated by ultrasonic

treatment on the workpiece was V_3, and the total relative velocity was $V_1+V_2+V_3$. The vibration caused the electrolyte to move rapidly to the spark discharge area. The number of ions participating in the MAO discharge per unit time increased, which effectively promoted the spark discharge and improved the microstructure and macroscopic performance of the coatings.

4. CONCLUSIONS

WO_3/Al_2O_3 composite ceramic coatings were prepared under ultrasound-enhanced MAO. The corrosion performance, hardness of the substrate was improved. The major conclusions are as follows:

1. The diameter of micro pores on the surface of coatings decreased with increasing Na_2WO_3 concentration. Meanwhile, the roughness decreased from 2.00μm to 1.67μm, and the coating thickness increased from 28.1μm to 39.3μm.

2. The coatings consisted of γ-Al_2O_3, α-Al_2O_3, and WO_3. The intensities of the peaks of γ-Al_2O_3 and WO_3 increased with increasing Na_2WO_3 concentration.

3. The corrosion current density was reduced from 32.59μA/cm^2 to 0.29μA/cm^2, and the hardness increased from 1025 HV to 1465 HV. The corrosion and hardness of the substrate was improved by ultrasound enhanced MAO and Na_2WO_3, providing a new way for expanding the applications of MAO technology in corrosive environments.

4. The vibration amplitude of the electrolyte increased to 140μm at 700W, and the ultrasound-enhanced MAO produced a high-frequency oscillation effect on the electrolyte, which promoted spark discharge and changing the microstructure of the coatings.

ACKNOWLEDGMENTS
This work was supported by the Introduce Talent Special Funding for Scientific Research at Nanjing Tech University (Grant No. 3827400212);

DISCLOSURE STATEMENT
No potential conflict of interest was reported by the authors.

References

1. S. Xin, L. Song, R. Zhao, X. Hu, *Thin Solid Films*, 515(2006)326-332.
2. Y. Yang, Y. Gu, L. Zhang, X. Jiao, J. Che, J. Mater. *Eng. Perform.*, 26(2017)6099-6106.
3. W. Shang, Y. Wang, Y. Wen, X. Zhan, D. Kong, *Int. J. Electrochem. Sci.*, 12(2017)11875-11891.
4. X.P. Zhao, D. Liu, J.Q. Lu, G.Y. Wei, *Int. J. Electrochem. Sci.*, 12(2017)7922-7930.
5. S.J. Ma, T.L. Wang, L.W. Qian, Z. Xiang, W. Lu, H.W. Yang, *Int. J. Electrochem. Sci.*, 13(2018)6451-6461.
6. D.X. Wang, X.W. Zhong, F.G. Liu, Z.N. Shi, *Int. J. Electrochem .Sci.*, 14(2019)9482-9489.
7. P. Wang, X.W. Wei, J. Pu, D. Xiong, J.W. Liu, Z.Y. Gong, J.Hu, W.J. Cao, X.T. Zu, *Int. J. Electrochem. Sci.,* 14(2019)5161-5173.

8. D.L. He, G.L. Li, D.J. Shen, C.H. Guo, H.J. Ma, J.R. Cai, *Vacuum*, 107(2014)99-102.
9. D.J. Shen, J.R. Cai, L.G. Li, D.L. He, L.L. Wu, H.J. Ma, Y.H. Xia, H. Chen, Y.Q. Yang, *Vacuum*, 99(2014)143-148.
10. L.J. Qu, M.Q. Li, M. Liu, E.L. Zhang, C. Ma, *J.Adv.Ceram.*,2(2013)227-234.
11. K. Wei, L. Chen, Y. Qu, Y. Zhang, X. Jin, W. Xue, J. Zhang, *Corros.Sci.*,143(2018)129-135.
12. S. Xie, Z. Bi, Y. Chen, X. He, X. Guo, X. Gao, X. Li, *Appl.Surf.Sci.*,459(2018)774-781.
13. Q. Chen, W. Li, K. Ling, R. Yang, *Materials&Design*, 190(2020)108558.
14. Y. Chen, J.H. Dou, Z.F. Pang, H.J. Yu, C.Z. Chen, J.K. Feng, *RSCAdv.*, 10(2020)8244-8254.
15. A. Hakimizad, K. Raeissi, M. Santamaria, M. Asghari, *Electrochim. Acta*, 284(2018)618-629.
16. M.R. Bayati, A.Z. Moshfegh, F. Golestani-Fard, R. Molaei, *Mater. Chem. Phys.*, 124(2010)203-207.
17. S.C. Di, Y.P. Guo, H. Lv, J. Yu, Z. Li, *Ceram. Int.*, 41(2015)6178-6186.
18. Y.P. Guo, S.C. Di, P.X. Lu, S.F .Sun, *RareMet. Mater. Eng.*, 44(2015)2240-2244.
19. Y.P. Guo, Z. Xue, G. Li, R.W. Xu, X.F. Lu, *Int. J. Electrochem. Sci.*, 15(2020)7682-7692.
20. M. Kaseem, Y.G. Ko, *J. Electrochem. Soc.*, 163(2016) C587-C592.
21. Q.Z. Chen, W.Z. Li, K. Ling, R.X. Yang, *Materials&Design*, 190(2020)14.
22. L. Chen, Y. Qu, X. Yang, B. Liao, W. Xue, W. Cheng, *Mater. Chem. Phys.*, 201(2017)311-322.
23. N.D. Charisiou, L. Tzounis, V. Sebastian, S.J. Hinder, M.A. Baker, K. Polychronopoulou, M.A. Goula, *Appl. Surf. Sci.*, 474(2019)42-56.
24. Y. Wang, D.B. Wei, J. Yu, S.C. Di, *J. Mater. Sci. Technol.*, 30(2014)984-990.
25. S. Sharma, S. Basu, Sep.Purif.*Technol.*, 231(2020)10.
26. H. Veisi, S. Razeghi, P. Mohammadi, S. Hemmati, *Materials Science&Engineering*, 97(2019)624-631.
27. A.P. Shpak, A.M. Korduban, M.M. Medvedskij, V.O. Kandyba, *J. Electron Spectrosc. Relat. Phenom.*, 156(2007)172-175.
28. L.J. Qu, M.Q. Li, M. Liu, M.H. Zhuang, C. Ma, E.L. Zhang, *Rare Met. Mater. Eng.*,43(2014)96-100.
29. Y. Wang, X. Zuo, D. Kong, Y. Zhou, *J. Mater. Res.*, 34(2019)3717-3724.
30. K. Yousefipour, A. Akbari, M.R. Bayati, *Ceram. Int.*, 39(2013)7809-7815.
31. E.V. Parfenov, A. Yerokhin, A. Matthews, *Surf. Coat. Technol.*, 203(2009)2896-2904.
32. X. Guo, K. Du, Q. Guo, Y. Wang, F. Wang, *ECS Electrochemistry Letters*, 2(2013)C11-C14.